Environmental Science Nano

ROYAL SOCIETY OF CHEMISTRY

PAPER

View Article Online
View Journal | View Issue

Cite this: *Environ. Sci.: Nano*, 2026, **13**, 2524

Interpreting the dynamic association of nanoplastics with *Chlorella vulgaris*: insight from single-cell analysis and Gaussian mixture modelling

Rega Permana, *[ab] Swati Sharma,[a] Bashiru Ibrahim, [ac] Tajudeen A. Oyehan,[a] Christopher Stark,[a] Miguel A. Gomez-Gonzalez, [d] Christian Pfrang [a] and Eugenia Valsami-Jones *[a]

Nanoplastics (NPls) have been recognized as emerging persistent toxic particulates in aquatic environments and their interactions with biota pose growing ecological concerns. Yet, the mechanisms governing their cellular association and resulting toxicity remain poorly resolved because population-level assays obscure the inherent variability among individual cells. Here, we integrate single-cell inductively coupled plasma mass spectrometry (SC-ICP-MS) with Gaussian mixture modelling (GMM) to quantify the dynamic heterogeneous association of Eu-doped polystyrene nanoplastics (Eu-doped NPls) with the model microalga *Chlorella vulgaris*. The GMM analysis identified distinct subpopulations exhibiting variable particle association that shift dynamically with exposure time and concentration. Across exposures of 5–20 mg L^{-1}, GMM analysis revealed that the majority of microalgal cells (35–65%) belonged to low-association clusters, whereas only a small fraction (0–10%) exhibited high NPls association, with pronounced temporal and concentration-dependent shifts in subpopulation structure. A generalized linear model (GLM) further demonstrated that these high-burden subpopulations disproportionately account for observed growth inhibition, increasing from 12.75% at 5 mg L^{-1} to 39.34% and 43.05% at 10 and 20 mg L^{-1}, respectively. Synchrotron-based nano X-ray fluorescence (nano-XRF) provided spatial evidence consistent with particle localization within or closely associated with algal cell, while physiological endpoints (chlorophyll-a content, CO_2 fixation, ROS, and MDA levels) validated the toxicity trends. This integrative single-cell and unsupervised machine-learning modelling framework provides quantitative evidence that stochastic, heterogeneous interactions underpin NPls toxicity in microalgae. The approach offers a transferable analytical paradigm for elucidating the fate and effects of persistent plastic pollutants in aquatic ecosystems.

Received 14th January 2026,
Accepted 20th April 2026

DOI: 10.1039/d6en00046k

rsc.li/es-nano

Environmental significance

Nanoplastic toxicity in aquatic systems is often assessed using population-level measurements, which can obscure important variability among individual cells. Using single-cell ICP-MS, this study reveals heterogeneous association of europium-doped polystyrene nanoplastics (Eu-doped NPls) within the freshwater microalga *Chlorella vulgaris*, a key primary producer in aquatic food webs. Unsupervised Gaussian mixture modelling identifies dynamically shifting cellular subpopulations with distinct NPls burdens. Generalised linear modelling further demonstrates that a small fraction of highly burdened cells disproportionately contributes to growth inhibition. By integrating single-cell measurements with data-driven analysis, this work provides new insight into how NPls interact with microalgal populations and highlights the importance of cellular heterogeneity in assessing the ecological risks of persistent NPls pollution.

1. Introduction

Discarded mismanaged plastic waste are prone to be exposed to physical and chemical degradation in the environment, eventually fragmenting into microplastics (MPls, <5 mm) and nanoplastics (NPls, <1 μm), both of which are increasingly categorized as persistence toxic substance (PTS).[1–4] Although not all plastics fully degrade to the nanoscale, fragmentation can generate extremely high particle numbers; for instance, a

[a] *School of Geography, Earth and Environmental Sciences, University of Birmingham, Edgbaston, Birmingham, B15 2TT, UK.*
E-mail: rxp286@student.bham.ac.uk, e.valsamijones@bham.ac.uk
[b] *Faculty of Fisheries and Marine Science, Universitas Padjadjaran, Jatinangor, Sumedang, 45363, Indonesia*
[c] *Department of Biochemistry and Molecular Biology, Faculty of Sciences, Sokoto State University, Sokoto State, 852101, Nigeria*
[d] *Diamond Light Source, Harwell Science and Innovation Campus, Didcot OX11 0DE, UK*

single consumer product has been shown to release up to 17 billion NPl particles.[5] Their nanoscale size gives NPls the ability to interfere with fundamental biological processes down to the cellular level, promoting bioaccumulation and a potential to reach humans through trophic transfer. This bioaccumulation may potentially generate a threat to human health through the consumption of aquatic-derived food products. For example, a recent study has reported that at least 2 mg of NPls is ingested annually by European citizens through seafood consumption.[6]

Microalgae are one of the most important unicellular organisms in aquatic ecosystems, as they are involved in many biogeochemical cycles and play a significant role as primary producers in the aquatic food chain. The impact of NPls exposure to microalgae has been recognised widely, ranging from growth inhibition, morphological damage, reduced photosynthetic ability as well as cellular oxidative stress.[7,8] However, there are limited studies addressing the quantitative association of NPls with microalgal cells, which is essential for elucidating the mechanistic link between particle–cell interactions and cellular toxicity. The lack of quantitative data is largely due to most conventional particle-tracking techniques struggling at the relevant size and concentration ranges of NPls.[9] Additionally, the inherent similarity of most plastic polymer materials to naturally occurring biochemicals such as proteins and biopolymers, adds to the difficulty of a practical determination of their impact.[10] Techniques such as fluorescence microscopy and flow cytometry rely on intrinsic or post-staining dyes prone to photobleaching, algal autofluorescence, and dye transfer, while vibrational spectroscopy (μ-FTIR, Raman) and bulk mass-spectrometric methods (Py-GC-MS, TG-GC-MS) provide polymer identification or quantification but lack the spatial resolution and single-cell sensitivity to reveal population heterogeneity.[11–13]

A practical way around this analytical limitation is to use metal-doped NPls. Embedding trace amounts of an element that has a minimum background in natural waters to the NPl particle, favours its detection using inductively coupled plasma mass spectrometry (ICP-MS). More importantly, coupling the same tracer concept to single-cell ICP-MS (SC-ICP-MS) allows counting of metal-labelled particles in individual cells. For instance, a recent study reported that more than 60% of *Pseudokirchneriella subcapitata* cells had an association with europium (Eu)-doped NPls after exposure for 72 h.[14] Another study revealed that *Cryptomonas ovata* and *Cryptomonas ozolini* cells associated with aggregates of palladium (Pd)-doped NPls.[15]

Heterogeneous cellular association profiles of nanoparticles (NPs), including NPls, where most cells internalise few or no particles while a minority accumulate disproportionately high loads, has been reported in a few recent studies.[16–18] Such sub-population variability is critical because cells with elevated intracellular particle content, even when they represent only a small fraction of the total cell count, could lead to population level effects.[19] At the same time, population-averaged measurements can hide the true toxic potential of NPls, underestimate hazard, and obscure mechanistic insight. Resolving these hidden subpopulations by combining SC-ICP-MS with data-driven clustering approach such as Gaussian mixture model (GMM) provides a more accurate picture of distribution, recognises cellular toxicity, and enables predictive models that link cellular heterogeneity to bulk-scale effects.

GMM is an unsupervised machine learning based on probabilistic clustering method that assumes the data are generated from a mixture of multiple Gaussian distributions, each representing a cluster. These clusters are interpreted as subpopulations that have a different level of NPls association on a per-cell basis. Unlike hard-threshold methods, GMM offers a flexible, data-driven approach that accounts for overlapping distributions and allows for soft classification of cells.[20] This is particularly advantageous for biological systems, where variability and heterogeneity are inherent, and where subpopulations may not be cleanly separable.[21,22] By modelling the distribution of association intensities, GMM enables more understanding of how NPls burden varies across individual cells and how these distributions evolve under different exposure conditions. The resulting subpopulation patterns can then be explored in relation to population-level growth inhibition *via* a generalised linear model (GLM).

Herein, a novel integrative single-cell framework was presented to elucidate the dynamic and heterogeneous association of NPls with microalgae cells. Europium doped polystyrene NPls (Eu-doped NPls) were used as the model NPls in this study, taking advantage of the low natural abundance of Eu and its high sensitivity detection by mass spectrometry. Polystyrene (PS) was purposively chosen since it is one of the most widespread plastics in the environment and is supported by substantial body of existing research.[23] The freshwater green algae *Chlorella vulgaris* (*C. vulgaris*) was chosen as a model unicellular organism due to its widespread ecological niche.[24,25] Single-cell mass-spectrometric quantification of Eu-doped NPls was integrated with Gaussian-mixture clustering (GMM) and generalized linear modelling (GLM) to decipher how distinct microalgal subpopulations relates to the overall growth-inhibition response. By supplying the first detailed quantitative cell-association for NPls in microalgae, this study adds critical knowledge and offers parameters that will improve understanding of risks posed by NPls pollution in the aquatic environment.

2. Materials and methods

2.1 Chemicals and reagents

All chemicals and reagents in this study were of analytical grade. Styrene (98%), potassium persulfate (KPS), sodium dodecyl sulfate (SDS), acetoacetyl methylmethacrylate (AAEM) europium(III) nitrate hydrate, hydrogen peroxide (H_2O_2, 30%), nitric acid (HNO_3, 70%), concentrated sulfuric acid (H_2SO_4), 2′,7′-dichlorodihydrofluorescein diacetate (H_2DCFDA), trichloroacetic acid (TCA), 2-thiobarbituric acid (TBA), glutaraldehyde solution (25%), bovine serum

albumin (BSA), phenol, and glucose were supplied from Sigma Aldrich (Gillingham, UK). Phosphate-buffered saline (10× PBS), ethanol (99.8%, analytical grade), and methanol (99.8%, analytical grade) were obtained from Thermo Fisher Scientific (Gloucester, UK). The Bio-Rad protein assay dye reagent concentrate was obtained from Bio-Rad (Watford, UK).

2.2 Microalgae cultivation

The green microalgae *C. vulgaris* (CCAP 211/11B) used in this study was obtained from Culture Collection of Algae and Protozoa (CCAP, UK). Cultures were grown in sterilized Bold's basal media (BBM), with the detailed composition provided in Table S1. Stock cultures were maintained in 1 litre (L) flasks and cultivated in a plant growth chamber at 22 °C under 4800 lux illumination with a 16 : 8 h light–dark cycle. Continuous aeration was provided by bubbling air through a 0.25 μm syringe filter (Whatman, UK) to keep the cells in suspension, and the flasks were shaken at least once daily to prevent sedimentation. Cell density was manually determined using a counting chamber under a light microscope. Additionally, the optical density (OD) of the cultures was measured at 680 nm using a UV-visible spectrophotometer (Shimadzu, Japan) and correlated linearly with cell density (R^2 = 0.99) to facilitate quantification (Fig. S1). Cultures were renewed every 6–7 days during the exponential phase to maintain the stock.

2.3 Eu-doped NPl characterisation in culture media

Eu-doped polystyrene NPls were synthesized by doping Eu into their structure, as described in a previous study[26] and provided in Text S1. In this synthesis batch, the Eu loading per particle was estimated by combining particle number measurements from single-particle ICP-MS (SP-ICP-MS) with bulk Eu mass quantification by ICP-MS. Eu-doped NPls were dispersed in deionized water (DIW) containing 0.1 wt% SDS to minimize particle aggregation. Suspensions were prepared at nominal concentrations of 5, 10 and 20 mg L^{-1} and sonicated in a bath sonicator for at least 40 min to ensure homogeneous dispersion. Each suspension was then divided into two aliquots: one for particle number determination by SP-ICP-MS and the other for complete digestion followed by ICP-MS analysis to quantify total Eu mass. The estimated Eu loading per particle was subsequently calculated by dividing the measured Eu mass concentration with the corresponding particle number concentration. Because this calculation is based on the Eu-bearing particle events detectable under the applied analytical conditions, the resulting value is interpreted here as an operational, event-based estimate for the analytically resolved particle population.

To assess the particle morphology, a stock solution (1000 mg L^{-1}) was prepared in DIW and stored at 4 °C. Transmission electron microscopy (TEM) was used to characterize the size and morphology of the Eu-doped NPls. To assess stability of Eu-doped NPls in BBM, the stock solution was diluted to 10 mg L^{-1} in BBM and aged for seven days under constant shaking (120 rpm) at room temperature (22 °C). Daily aliquots were analysed for hydrodynamic size and zeta potential using dynamic light scattering (DLS) with a Zetasizer Nano ZS (Malvern Instruments Ltd., UK). Measurements were performed using disposable cuvettes with approximately 1 mL sample volume, and samples were analysed without dilution. Hydrodynamic size was determined from seven independent replicates with 20 runs per replicate, while zeta potential measurements were conducted in triplicate with 50 runs per replicate. Additionally, Eu leaching was monitored by filtering aliquots through a 20 nm Whatman syringe filter, followed by leached Eu quantification using ICP-MS analysis.

2.4 Experimental setup

The toxicity of Eu-doped NPls to *C. vulgaris* cells was evaluated using an algal growth inhibition test based on OECD 201 guidelines with slight modifications.[27] In brief, Eu-doped NPls were first dispersed in 250 mL of sterile BBM in Erlenmeyer flasks to achieve final concentrations of 5, 10 and 20 mg L^{-1}. These concentration ranges simulate a scenario in which NPl levels could increase up to 10^{14} times the current concentration of MPls and to enable mechanistic investigation and ensure sufficient signal for single-cell analytical detection.[28] Prior to the growth inhibition test, each flask was sonicated for at least 10 minutes to ensure homogeneous dispersion. Pre-cultured *C. vulgaris* cells in their exponential phase were then inoculated into each flask, including the negative control (without Eu-doped NPls), at an initial cell density of 1×10^6 cells per mL. The growth inhibition test was performed over a 72 h period in a growth chamber maintained at 22 °C under 4800 lux illumination and a 16 : 8 h light–dark cycle. First order nonlinear kinetic model was used to assess the cells growth rate under different range of Eu-doped NPls concentration and inhibition rate (IR) was calculated by comparing the cells count to control group (Text S2).

2.5 Determination of cellular association using ICP-MS and SC-ICP-MS

The uptake of Eu-doped NPls by microalgal cells was quantified by measuring the amount of Eu in the supernatant (representing the remaining NPls) and pellet (representing the biomass of *C. vulgaris*) using ICP-MS in KED mode and in individual cells (representing associated Eu-doped NPls) using SC-ICP-MS. Measurements were conducted at 24, 48 and 72 h for each treatment. Briefly, biomass from each experimental flask was collected at each sampling time and centrifuged at 3600*g* for 10 min. The supernatant was then collected and digested with concentrated nitric acid for quantification of the remaining Eu-doped NPls using ICP-MS (PerkinElmer Inc., UK); detailed digestion protocols can be found in Text S3. The cell pellet

was washed three times with 10× PBS to remove any loosely bound Eu-doped NPls and subsequently resuspended in 10 mL of 10× PBS. The obtained cell pellet was digested to determine the bulk Eu-doped NPl association and partly redispersed in DIW for further SC-ICP-MS analysis (PerkinElmer Inc., UK). The number of cells detected by SC-ICP-MS was compared to the total cell count obtained manually using counting chamber, following established algal enumeration methods.[14] Detailed operational parameters for both ICP-MS and SC-ICP-MS are provided in Tables S2 and S3, respectively.

Eu events in SC-ICP-MS were identified using a 3σ threshold above the background signal, where the event threshold was defined as the mean background signal plus three times the standard deviation of the baseline noise, following commonly used event-discrimination approaches in SC- and SP-ICP-MS.[29–31] Under the acquisition conditions used in this study, this corresponded to a signal threshold of 1.01 counts per dwell, which was applied to distinguish true Eu events from background fluctuations. The mass-equivalent detection limit for Eu was then estimated by converting the instrumental signal threshold to mass using the calibration slope applied in the SC-ICP-MS data processing workflow.[32] Based on this approach, the event-level detection limit was estimated to be approximately 45 ag Eu per event. The detailed calculation is provided in Text S4.

2.6 Computational and statistical modelling

To resolve heterogeneity in single-cell association data, Gaussian mixture models (GMM) were applied to Eu mass distributions obtained from SC-ICP-MS. The optimal number of clusters/subpopulations was determined by the Bayesian information criterion (BIC), and cluster weights were used to describe the relative abundance of subpopulations across exposure conditions. To link subpopulation structure with population-level toxicity, a generalised linear model (GLM) was developed using dose, exposure time, and selected GMM-derived cluster proportions as predictors of growth inhibition. Model quality was evaluated by Akaike information criterion (AIC), root-mean-square error (RMSE), and pseudo-R^2. All modelling and visualization were performed in R (version 4.5.0) using mclust and glm packages. Detailed parameter settings, and diagnostics are provided in Text S5 and S6.

2.7 Synchrotron-based nanoscale X-ray fluorescence imaging

For detailed nanoscale elemental mapping and chemical imaging, synchrotron radiation X-ray fluorescence (nano-XRF) was employed to probe the Eu localization within the cells exposed to Eu-doped NPls. In this study, fixed and dehydrated samples were prepared by mounting them onto 5 × 5 mm^2 silicon nitride (Si_3N_4) membranes (Silson Ltd., Warwickshire, UK). XRF scanning was then performed at the I14 Hard X-ray Nanoprobe beamline at Diamond Light Source (UK) using a finely focused 50 × 50 nm beam, an incident energy of 9 keV, and a four-element silicon drift detector (SGX-Ray Spec, UK), as described elsewhere.[33] High-resolution XRF maps were acquired by raster scanning the sample through the X-ray focus, using a 50 nm step size with 15 ms dwell time over 10 μm size areas. The PyMca suite was employed for batch fitting and pixel-by-pixel background subtraction, and additional image processing was performed using ImageJ software.[34]

2.8 Growth and physiological endpoint analysis

2.8.1 Determination of chlorophyll-a and CO_2 uptake rate. To evaluate the photosynthesis performance of the Eu-doped NPls-exposed and unexposed *C. vulgaris* cell, chlorophyll-a (Chl-a) determination was performed following previously described protocols using a methanol extraction method.[35] The Chl-a was recorded daily at 24, 48 and 72 h. Accordingly, at the end of exposure test, CO_2 uptake rate was also determined by measuring the productivity of the biomass and elemental carbon.[36,37] The detailed protocol for both Chl-a measurement and CO_2 uptake is outlined in Text S7 and S8.

2.8.2 Cellular stress and soluble EPS biochemical responses. Intracellular reactive oxygen species (ROS) was measured at 24, 48 and 72 h using the fluorescent dye H_2DCFDA and reported as percentage by comparing to control.[38] The complete protocols for ROS measurement provided in Text S9. Lipid peroxidation was determined by measuring malondialdehyde (MDA) equivalents at 24, 48, and 72 h (Text S10), according to a previously described method.[39] Here, soluble EPS were quantified as dissolved organic carbon (DOC) using a TOC analyzer (Model TOC-L, Shimadzu).[40] Additionally, the protein content of the soluble EPS was measured using the BSA assay,[41] and the carbohydrate content was determined using the phenol-sulphuric acid assay.[42] The detailed procedure for soluble EPS measurement and protein-to-carbohydrate ratio is described in the Text S11. ATR-FTIR (PerkinElmer Inc. Instruments, UK) was further used to examine the changes in surface chemistry of the exposed and unexposed cells (Text S12). To complement the results, at the end of the exposure test, scanning electron microscope (SEM) (Carl Zeiss Inc., UK) analysis was performed to examine changes in the morphology of microalgal cells upon exposure to Eu-doped NPls (Text S13).

2.9 Statistical analysis

Data normality was assessed using the Shapiro–Wilk test. Statistical comparisons were performed using one-way analysis of variance (ANOVA) for parametric data or the Kruskal–Wallis test for non-parametric data, both at a 5% significance level. Statistical analyses were conducted using SigmaPlot 15.0. Cluster analysis (subpopulation) and its link to growth inhibition were modelled using Gaussian mixture model (GMM) and generalised linear model (GLM) using R (v4.5.0). Pearson correlation of pixel-wise nano-XRF data

was conducted to analyse the elemental colocalization using R (v4.5.0).

3. Results and discussion

3.1 Eu-doped NPls characterization in Bold's basal media (BBM)

The synthesis batch of Eu-doped NPls produced particles with consistent Eu incorporation. Based on combined SP-ICP-MS particle number measurements and bulk Eu quantification by ICP-MS after digestion, the calculated Eu content was 0.86 ± 0.06 μg Eu per mg NPls, corresponding to an estimated Eu loading of 13.02 ± 2.68 ag Eu per particle. This estimate is directly linked to the Eu-bearing particle events resolved by SP-ICP-MS and is therefore used here as the primary analytical estimate of particle-associated Eu loading. The calculation procedure used to estimate Eu content and per-particle loading is summarized in Table S4.

To assess the particle behaviour in exposure media, Eu-doped NPls were characterized in BBM over a period of 7 days. A schematic overview of the particle system is shown in Fig. 1A, illustrating the polymeric matrix with doped Eu tracer. TEM revealed spherical, monodisperse particles with moderate agglomeration (Fig. 1B), with a mean particle diameter of 31.94 ± 4.17 nm (inset). DLS measurements revealed that the Eu-doped NPls exhibited moderate agglomeration upon dispersion in BBM, with

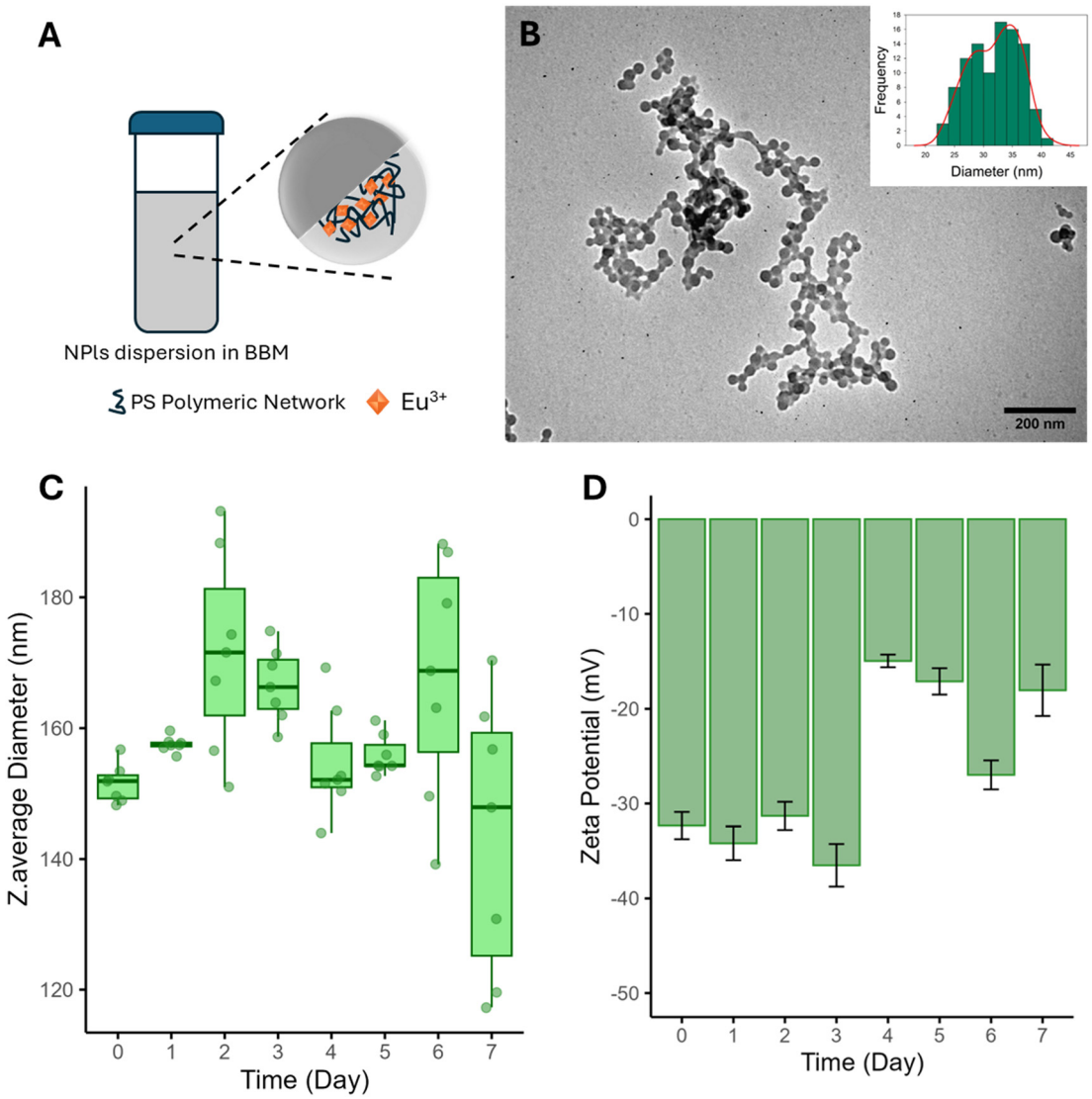

Fig. 1 Characterization of Eu-doped NPls in BBM. (A) Schematic illustration of the Eu-doped NPls system used in this study. Particles consist of a polymeric matrix embedded with Eu tracer, enabling multimodal detection. (B) TEM image showing spherical NPls with moderate aggregation. Inset: Size distribution histogram based on particle diameter measurements (n = 100), fitted with a Gaussian curve. (C) Changes in hydrodynamic diameter of Eu-doped NPls over 7 days in BBM. Data presented as box plots with individual data points (n = 7). (D) Temporal changes in zeta potential (mV) of Eu-doped NPls in BBM. Plot graphs represent mean ± standard deviation (SD) (n = 3).

hydrodynamic diameter ranging from 151.55 ± 2.74 nm to 171.75 ± 14.24 nm over the period of 7 days (Fig. 1C). This increase in size reflects weak interparticle interactions and ionic strength effects in BBM. The discrepancy between the primary particle size and the larger hydrodynamic diameter can be explained by partial aggregation in suspension and methodological differences where DLS measures the solvated, intensity-weighted hydrodynamic size, including any loosely bound corona, whereas TEM is performed under high vacuum, so the hydration layer collapses and only the dry-state core is imaged.

Simultaneously, the zeta potential values varied from −14.94 ± 0.94 mV to −36.5 ± 2.01 mV (Fig. 1D) but generally remained predominantly negative over the 7 days period in BBM, indicating stable colloidal dispersion. However, a slight decrease in magnitude after day 3 suggests potential surface modification, aggregation, or interaction with media components over time, which was due to the existing K^+, Na^+, Ca^{2+}, Mg^{2+} and PO_4^{3-} in the medium. As these ions diffuse into the electrical double layer, they compress the Debye length and screen surface charge, invariably pushing the charge toward zero. Additionally, no measurable release of Eu was detected over the 7 days exposure period, confirming that the Eu remained securely encapsulated within the PS polymer matrix. This further confirmed that Eu-doped NPls remained suspended and colloidally stable during the exposure period, enabling reliable interaction with microalgal cells in subsequent toxicity assays.

3.2 Eu-doped NPls association with *C. vulgaris* cells

3.2.1 Accumulation of Eu-doped NPl in *C. vulgaris*. A first-order nonlinear kinetic model revealed that the growth rate of *C. vulgaris* decreased with increasing Eu-doped NPl concentrations, showing a clear dose-dependent inhibition trend (Fig. S2A and B). No growth inhibition above 50% was observed in this study, which aligns well with the reported 72 h EC_{50} of 19.9 mg L^{-1} for 50 nm NPls against *C. vulgaris*.[43] The bulk weight of NPls accumulated in the *C. vulgaris* biomass was then estimated from the linear mass correlation between Eu and NPls (R^2 = 0.99) (Fig. S3A). The exposure concentrations used in this study (5–20 mg L^{-1}) correspond to approximately 3.7×10^{11}–1.8×10^{12} particles L^{-1}, based on the particle number calibration obtained from SP-ICP-MS measurements (Fig. S3B). These concentrations are higher than currently reported environmental estimates for NPl in aquatic systems. However, elevated concentrations were intentionally employed in this study to facilitate measurable NPl–cell interactions under controlled laboratory conditions and to enable statistically robust single-cell ICP-MS analysis, as commonly applied in mechanistic nanoparticle exposure studies.[44] The concentration of Eu-doped NPls in digested

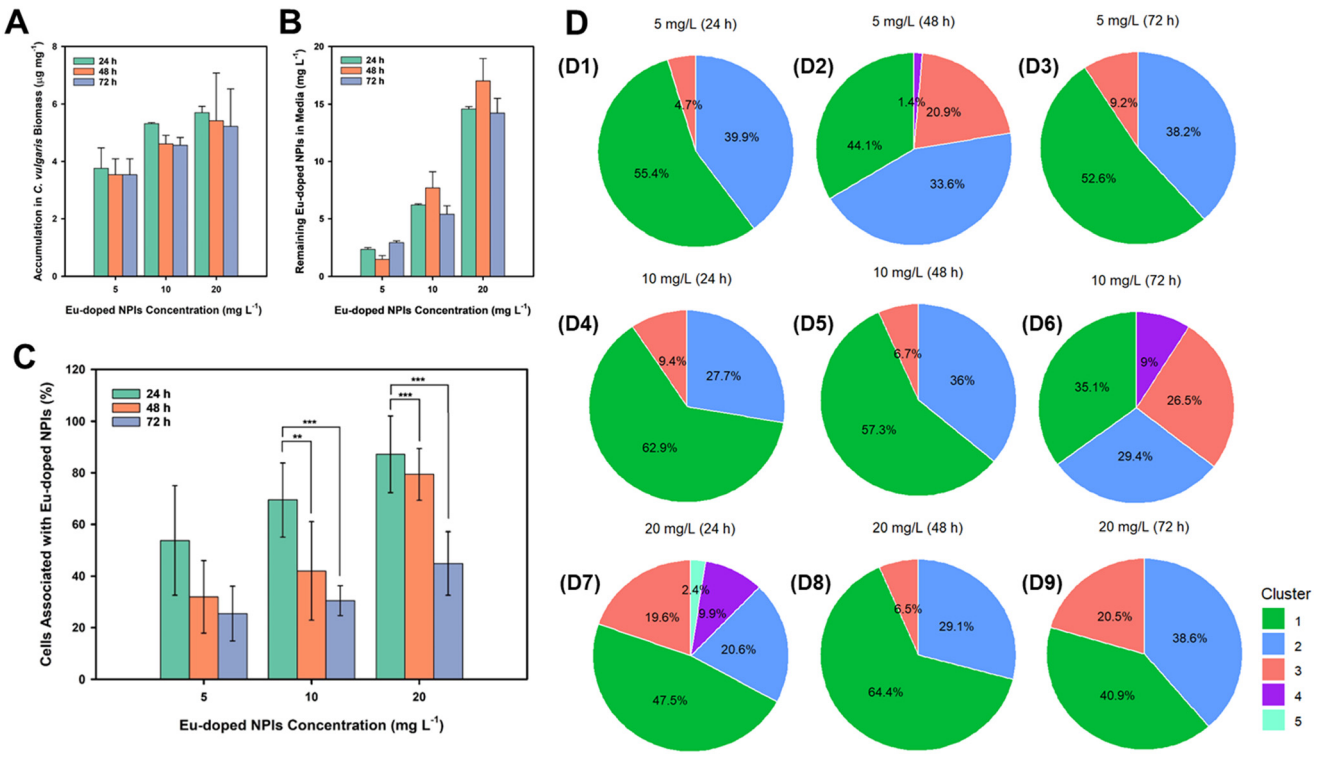

Fig. 2 Bulk and cellular association of Eu-doped NPls with *Chlorella vulgaris*. (A) Total Eu-doped NPls concentration measured in pellet and (B) supernatant of *C. vulgaris* during exposure, obtained by measuring Eu using ICP-MS. (C) The proportion of cells associated with Eu-doped NPls obtained by SC-ICP-MS relative to whole cell population manually counted using counting chamber. (D) The weight proportions of each cluster derived from GMM based on Eu mass distribution recorded from SC-ICP-MS. D1–D9 are arranged by concentration from top to bottom (5, 10, and 20 mg L^{-1}) and exposure time from left to right (24, 48, and 72 h). Plots graphs represent mean ± SD (n = 3). Bars with an asterisk indicate statistically significant differences (* = $p < 0.05$, ** = $p < 0.01$, *** = $p < 0.001$) using one-way ANOVA followed by *post hoc* multiple comparison testing.

C. vulgaris cells pellet and supernatant during growth inhibition test is shown in Fig. 2A and B. The calculated recovery rate of Eu-doped NPls was ranged from approximately 84% to 122% across the different exposure conditions and time points (Table S5), which falls within the range commonly reported for nanoparticle mass balance measurements.[45]

A relatively consistent proportion (50–70%) of the Eu-doped NPls remained freely dispersed in the media, suggesting that only one-third of Eu-doped NPls associated to the algae in bulk. Interestingly, despite the ongoing cell division and the continued presence of unbound NPls in the supernatant, the biomass-normalised NPl burdens in the pellet (3.5–5.7 μg mg^{-1}) indicated an apparent decreasing trend, although this trend was not statistically significant. This suggests that newly formed cells did not substantially increase overall particle uptake, potentially due to cellular physiological responses involving enhanced soluble EPS release, as evidenced by the statistically significant increase in dissolved organic carbon (DOC) in the supernatant across all concentrations and time points (Fig. S4A), reflecting elevated soluble EPS production. The soluble EPS composition also shifted in response to exposure, as reflected by an elevated protein-to-carbohydrate (P/C) ratio (Fig. S4B), indicating a metabolic reallocation towards proteinaceous soluble EPS components that may chelate or bind Eu-doped NPls. Secreted soluble EPS is often the first to interact with foreign materials leading to stabilization (*e.g.* through bio-corona formation), aggregation and sedimentation of the particle, making it less available for the newly divided cells.[46]

3.2.2 Quantitative association analysis using single-cell ICP-MS. Following bulk-phase analysis, SC-ICP-MS was used to resolve the extent and variability of Eu-doped NPl association across individual algal cells. In this approach, Eu events detected during SC-ICP-MS measurements were interpreted primarily as arising from cell-associated Eu-doped NPls. To evaluate the potential contribution of soluble EPS to Eu-doped NPls aggregation, a control experiment was performed in which Eu-doped NPls were incubated with cell-free algal filtrate. After 24 h, the *z*-average particle size increased significantly compared to suspensions in DIW and BBM (Fig. S5A), indicating that soluble EPS can promote particle aggregation. However, sequential washing performed on a representative exposure condition showed that most loosely associated Eu-doped NPls were removed during the first PBS wash, while negligible concentrations were detected in the second and third washes (Fig. S5B), indicating effective removal of weakly bound particles prior to analysis. Therefore, while EPS-induced aggregation may occur in the exposure medium, the contribution of free aggregates to the detected Eu events is expected to be minimal. Accordingly, SC-ICP-MS signals are interpreted conservatively as reflecting primarily cell-associated Eu-doped NPls.

Control measurements were performed to evaluate potential background Eu signals. Algal suspensions without Eu-doped NPls produced no detectable Eu events, confirming that algal cells themselves do not generate Eu spikes under the measurement conditions. In addition, a particle-only suspension analysed under identical SC-ICP-MS conditions produced only a very small number of Eu events (<5 events per acquisition; Fig. S6).

This observation is consistent with the estimated Eu loading of the particles (13.02 ± 2.68 ag Eu per particle), which is below the calculated SC-ICP-MS event detection limit of 45 ag per event in this study. On this basis, individual free-floating Eu-doped NPls would not be expected to generate resolvable single-particle events, and the few detected events in the particle-only control are more likely to reflect transient aggregates or coincident entry of multiple particles into the plasma. In contrast, samples containing exposed algal cells generated hundreds to thousands of Eu events, supporting the interpretation that most Eu events detected in the exposure experiments arose from cell-associated Eu-doped NPls, although a minor contribution from residual particle aggregates cannot be completely excluded.

The recorded cells number from the instrument indicated number of cells positively contained Eu-doped NPls. This cell number was then normalized to the whole population number obtained *via* manual cells counting chamber.[14] The data revealed that Eu-doped NPls association with *C. vulgaris* cells were both dose- and time-dependent (Fig. 2C). At 5 mg L^{-1}, roughly 53% of cells carried detectable Eu at 24 h, but that fraction fell to 25% by 72 h. At 10 mg L^{-1} the initial association was higher (69%) and likewise dropped to 31% by 72 h, while at 20 mg L^{-1} a very large fraction (87%) of cells was Eu-positive at 24 h, decreasing to 45% after 72 h. Similar results have been reported for nanoparticle (NP) association with cells, for instance, in a previous study less than 50% of *Pseudokirchneriella subcapitata* cells were associated with gold NPs after 72 h.[47] Note that the SC-ICP-MS revealed the cumulative association of NPls with the cells, which included the tightly bound NPls as well as NPls that internalized into the cells.

This continuous reduction of the proportion of Eu-doped NPls associated cells can be explained by the growth dilution effect of cell–particle over time. In actively dividing cells, any associated particles would be partitioned between daughter cells, suggesting that the particle load per cell is theoretically halved in each generation.[48] Although this phenomenon has not previously been demonstrated in microalgae, analogous mitotic dilution effects have been reported in other biological systems and for different nanomaterials. Recent studies showed that the uptake of NPls to human colorectal cancer cell lines (HCT116) decreased after prolong exposure (up to 7 days) implying that cell proliferation outnumber the constant particle concentration.[49] This classical mitotic dilution has been also observed in other studies examining other NPs loading in cells. A study exposing silica NPs to human lung fibroblasts (WI-38) showed a gradual decreased of total accumulated particle in proliferating cells while in

senescence (cell-cycle arrested), the cells loading remained unchanged.[50] Collectively, their findings emphasized that cell division leads to redistribution of particle between each generation, creating the wide cell-to-cell variance on a stochastic association.[16,47,51] This suggest that growth dilution associated with cell division may also contribute to heterogeneous NPls association dynamics in microalgae.

3.2.3 Modelling the subpopulation of cells associated with Eu-doped NPls using Gaussian mixture model (GMM). The Eu mass measured in a single event of SC-ICP-MS corresponds to an individual algal cell, recorded as a function of elemental mass distribution. Based on this dataset, a Gaussian mixture model (GMM) was applied using an expectation–maximization (EM) algorithm to identify distinct clusters within the Eu-doped NPl-associated cell population. The estimated proportion of each subpopulation across sampling time points and nominal exposure concentrations is presented in Fig. 2D. The detailed model summary and evaluation, including fitting diagnostics and classification metrics, are provided in the Table S6 and Fig. S7.

The model consistently identified at least three subpopulations of associated cells across all doses and time points, with two additional subpopulations appearing under certain conditions. These were categorized by increasing Eu mass depicting: subpopulation 1 (very low), subpopulation 2 (low), subpopulation 3 (moderate), subpopulation 4 (high), and subpopulation 5 (very high), as seen in density plot (Fig. S8). Most associated cells belonged to subpopulation 1, suggesting that most algal cells carried only a small quantity of Eu-doped NPls. In contrast, the subpopulation 5 appeared only at the highest exposure concentration (20 mg L^{-1}) after 24 h, indicating a supply-driven association mechanism where elevated particle availability increases the likelihood of early cell–particle interactions.

To provide an approximate interpretation of the Eu signals in terms of particle burden, the mean Eu mass associated with each GMM-derived cluster was converted to particle equivalents per cell using the estimated average Eu loading of the synthesized Eu-doped NPls. Across treatments, the cluster mean masses spanned approximately 50 to 2650 ag Eu per cell, corresponding to roughly 4 to 200 particle equivalents per cell, indicating substantial heterogeneity in NPls association among individual cells. An order-of-magnitude estimation indicates that even in the highest-burden subpopulation, the total volume of associated Eu-doped NPls represents only a very small fraction of the algal cell volume ($\sim 10^{-4}$%), assuming an algal cell size of 3–5 μm and an individual Eu-doped NPls size of 31.94 ± 4.17 nm. This suggests that the observed particle burden is not physically inconsistent with intracellular accommodation, although spatial localisation cannot be resolved by SC-ICP-MS. Because the GMM represents a soft-clustering approach, these components should be interpreted as overlapping modes within a continuous distribution of Eu burdens rather than discrete cellular classes. Consequently, the derived particle-equivalent values should be interpreted as approximate association burdens rather than exact particle numbers per cell. A summary of the corresponding Eu mass ranges and their approximate particle-equivalent burdens in each subpopulation is provided in Table S7.

Based on the observed decline in total associated cells over time, a rise in the low content (subpopulation 1) was initially expected, consistent with the growth dilution hypothesis. As dividing cells inherit internalized particles, the per-cell load should theoretically decrease, shifting the distribution toward lower mass clusters. However, the GMM analysis did not show a significant increase in subpopulation 1 over time. This may be explained by asymmetric inheritance of the Eu-doped NPls and the generation of particle-free daughter cells, which fall below the SC-ICP-MS detection threshold and are not included in the clustering.[48]

Interestingly, an increase in the high-content subpopulation (subpopulation 3) was observed after 72 h in the 10 and 20 mg L^{-1} treatments, despite an overall reduction in the fraction of associated cells. This suggests that a subset of cells either remained actively loaded or encountered localized concentrations of Eu-doped NPls later in the exposure period. Such findings point to a dynamic and heterogeneous pattern of cell–particle interaction, where particle association is governed not only by dose and time but also by physiological variability within the algal population. These GMM-derived trends highlight the dynamic and heterogeneous nature of NPl association over the 72 h exposure period. To our knowledge, this is among the first studies to quantitatively describe dynamic subpopulation shifts in NPl-associated algal cells at the single-cell level.

3.3 Linking subpopulation profiles to toxicity with generalized linear model (GLM)

For better understanding of the relationship between subpopulation profiles and the outcome toxicity at population level, an exploratory GLM was developed. This model combines the predicted interrelations outcome of dose, time and subpopulation on growth inhibition. The goal is to find whether some subpopulation has influence on the inhibition observed at population level. While a full GLM including all identified clusters were initially considered, comparative model evaluation based on AIC, RMSE, and pseudo-R^2 indicated that a reduced model including only subpopulation 1 (low association) and subpopulation 3 (high association) provided better predictive performance (Table S8). This reduced GLM was therefore selected for further analysis because it provided the best overall fit among the tested pairwise modes and offered an interpretable framework for exploring link between subpopulation structure and growth inhibition.

The predicted growth inhibition with the actual observed values of the reduced GLM with subpopulation 1 and 3 is shown in Fig. 3A. The observed and predicted inhibition

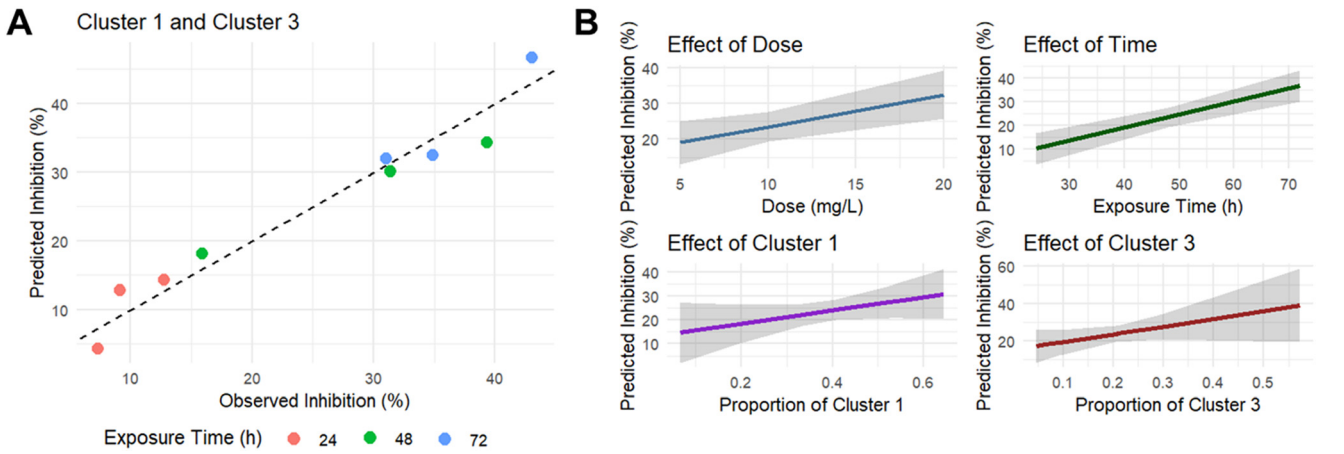

Fig. 3 Reduced GLM of growth inhibition as a function of NPls exposure and cell subpopulation structure. (A) Observed *versus* predicted algal growth inhibition (%), modelled using dose, exposure time, and proportions of cluster 1 and cluster 3 (identified *via* Gaussian mixture model of SC-ICP-MS data). Data points are color-coded by exposure time (24 h in red, 48 h in green, and 72 h in blue). (B) Partial effects of individual predictors on predicted growth inhibition. Shaded regions represent 95% confidence intervals (CI).

values showed close agreement around the 1:1 line, indicating that the reduced model captured a substantial proportion of the variation in growth inhibition (r^2 = 0.9; RMSE 2.9). Dose and exposure time were positively associated with growth inhibition in the reduced model, with both predictors showing statistically significant effect. The model estimated that every 1 mg L^{-1} increase in Eu-doped NPl concentration will increase the growth inhibition 0.89% and every hour extent in the exposure time will give 0.55% inhibition. Although the coefficients for subpopulation 1 (0.105) and 3 (0.088) did not reach conventional statistical significance, their positive effect estimates were retained in the best performing model and may indicate an exploratory association between subpopulation structure and growth inhibition, so it should not be dismissed completely.[52,53] The larger positive coefficient estimated for subpopulation 3, relative to subpopulation 1, is consistent with a stronger association between higher-burden cells and growth inhibition, although this pattern should be interpreted cautiously. Together, these results are consistent with the hypothesis that higher-burden subpopulation may contribute more strongly to the observed inhibition whereas low-burden cells may reflect weaker or sub-lethal responses.

The predicted outcome of growth inhibition in relation of changing variables of dose, exposure time and the proportion of subpopulation 1 and 3 with their respective CI (grey area around the line) is shown in Fig. 3B. The effect-plots showed that growth inhibition in *C. vulgaris* rises linearly with both Eu-doped NPls dose and exposure time, confirming the classical dose- and time-dependent toxicity reported for polymeric and metal-oxide NPs in previously reported studies.[48,50] The model reveals a pronounced contribution as the proportion of subpopulation 3 rises to 50%, predicted inhibition almost doubles, underscoring the role of heavily loaded hot-spot cells in driving population-level toxicity. In contrast, the low-burden subpopulation shows only a modest and uncertain effect. Together, the plots support a two-tier mechanism: (i) dose and time establish the external exposure pressure, (ii) toxicity is amplified by a minority of uptake-competent cells that accumulate large particle loads, an effect of high-accumulating cell dominance that has been recently recognized for variety of NP.[17,18,54] These findings highlight the importance of coupling bulk measurements with single-cell statistics to capture the heterogeneous and non-linear nature of particle–cell interactions.

3.4 Nanoplastic association and distribution *via* nano-XRF mapping

To illustrate the association of algal cells with Eu-doped NPls, nano-XRF maps of microalgae exposed to 10 mg L^{-1} Eu-doped NPls exposure treatment (Fig. 4A–H) were carried out, and its corresponding fitted XRF spectrum from PyMca analysis (Fig. 4I) was presented. Synchrotron nano-XRF was employed because it provides sub-micron spatial resolution and high sensitivity for trace elements, enabling elemental mapping at the scale of individual cells. Compared with conventional techniques such as LA-ICP-MS or SEM-EDS, synchrotron-based XRF allows higher spatial resolution and improved detection of low-abundance tracer elements such as Eu in biological samples.[55,56] The 10 mg L^{-1} concentration was selected as it produced the most distinct and robust Eu signal, indicative of Eu-doped NPls localization while control cells showed no Eu signal as confirmed by the PyMca fitting (Fig. S9). Based on the 10 × 10 μm scan area and the 2–3 μm Eu-rich region, the elemental maps likely represented a single *C. vulgaris* cell. While the broader field of view may contain additional cellular material or extracellular signal, the spatial coincidence of elemental signals within the mapped region is consistent with this interpretation.

Chlorella vulgaris cells typically range from 2–10 μm in diameter, although the nano-XRF maps presented here

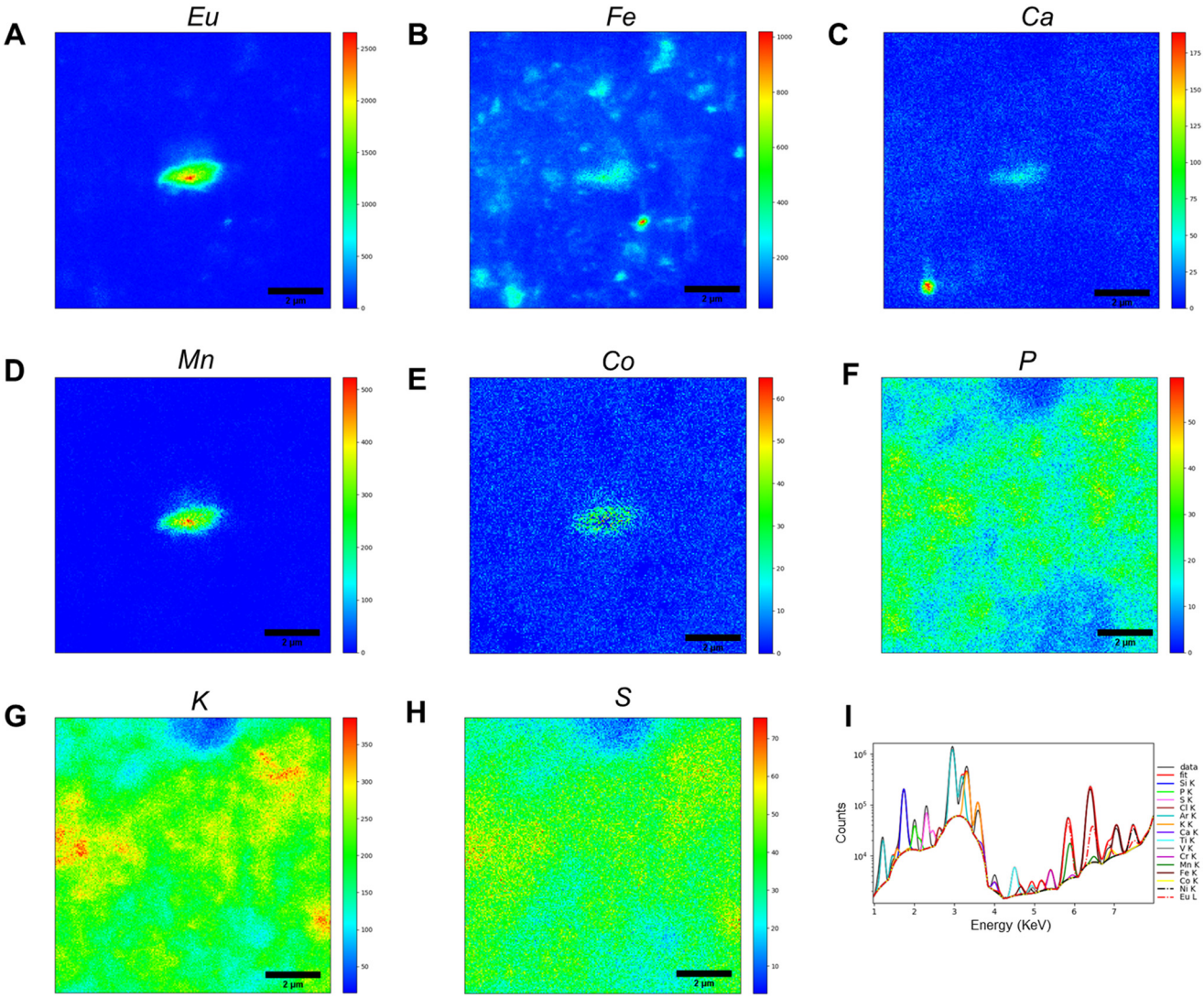

Fig. 4 Representative synchrotron nano-XRF elemental maps of a *C. vulgaris* cell exposed to Eu-doped NPls. (A–H) Spatial distribution of a specific element, with warmer colours indicating higher concentration or fluorescence intensity. (I) Fitted XRF spectrum for the region, verifying peak assignments.

primarily reflect elemental distributions and do not provide sufficient morphological contrast to delineate the cell boundary clearly. The bright Eu hotspots therefore indicate localized accumulation or association of Eu-doped NPls rather than the full cellular extent. The Eu signal forms an approximately circular or oval region 2–3 µm in diameter, suggesting that Eu-doped NPls were concentrated within a localized region of the mapped cellular are. Notably, Eu was not spread uniformly throughout the cell, instead it appeared in a clustered accumulation. The field suggested that some neighbouring cell or debris had P and other elements but negligible Eu. This implied cell-to-cell variability in NPls association, where some cells accumulate significant amounts of the particles while others may not. Such heterogeneity could arise from differences in cell physiological state and the stochastic contact with the particulate contaminants.

Pixel-wise analysis indicated positive correlations between Eu and several biologically relevant elemental markers, particularly Mn and Fe ($r^2 = 0.863$ and $r^2 = 0.846$, respectively; $p < 0.001$) across four regions of interest (Fig. S10). Algal cells naturally contain Mn and Fe as essential micronutrient involved in photosynthetic processes and various enzymatic functions.[57] In some regions, Eu hotspots appeared spatially proximal to Mn and Fe enriched areas, suggesting that Eu-doped NPls may associate with regions enriched in these biologically relevant metals. However, the degree of spatial coincidence varied among different ROIs, indicating heterogeneous relationships between Eu hotspots and cellular elemental distributions. Additionally, a weaker Eu–Ca correlation ($r^2 = 0.303$, $p < 0.001$) suggests that part of the Eu signal may also be associated with Ca-rich cell surface structure. Together, these observations indicate that Eu-doped NPls may interact with algal cells through

combination of surface association and possible intracellular localisation. Nevertheless, given the two-dimensional nature of nano-XRF maps, definitive discrimination between surface attachment and internalisation would require further techniques, such as three-dimensional imaging approaches.

The observed elemental association suggests that Eu-doped NPls may occur in regions enriched in metals (Fig. S11). Biologically, such elemental environments may correspond to intracellular compartments where algae regulate metal homeostasis, such as vacuole-like structures.[58] However, since the nano-XRF only provides two-dimensional projected elemental maps, these observations should be interpreted cautiously and do not provide definitive evidence of intracellular localisation. Previous studies have reported internalisation of nano-sized particles in microorganisms, including observation of NPls within *Chlamydomonas reinhardtii*,[59] which may provide a possible explanation for the spatial patterns observed here. Additionally, SEM imaging revealed attachment of Eu-doped NPls-EPS network on the surface of the *C. vulgaris* cells (Fig. S12). The presence of visible attachment was further exacerbated as the exposure concentration increased. Collectively, these data demonstrate that Eu-doped NPls may associate with algal cells both at the surface and potentially within cellular regions.

3.5 Eu-doped NPls toxicity to *Chlorella vulgaris*: physiological endpoint analysis

3.5.1 Photosynthesis and carbon uptake. To further understand the growth impact resulting from the Eu-doped

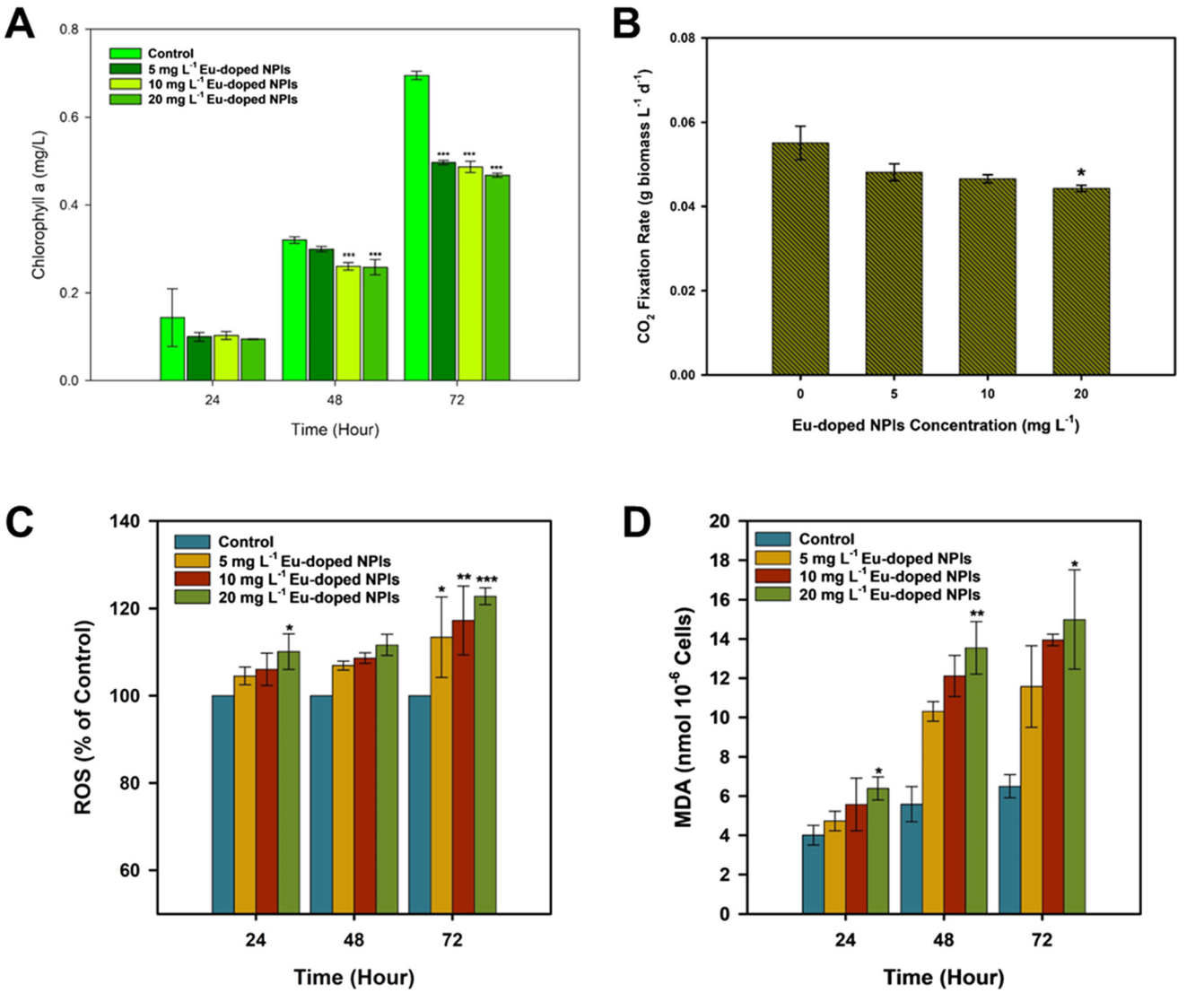

Fig. 5 Physiological endpoints analysis of *C. vulgaris* during 72 h growth inhibition test. (A) Daily changes of chlorophyll-a concentration during 72 h inhibition test (asterisk sign shows significance level compared to control). (B) CO_2 fixation rate at the end of 72 h inhibition test. (C) Intracellular ROS production relative to control (D) lipid peroxidation expressed by MDA level generated plot graphs represent mean ± SD (n = 3) and bars with an asterisk indicates statistically significant difference (* = $p < 0.05$, ** = $p < 0.01$, *** = $p < 0.001$) when compared to control using Kruskal–Wallis test.

NPls exposure, Chl-a, a photosynthesis biomarker was characterized. Chl-a trends capture how the growth change induced by the Eu-doped NPls ultimately translating into physiological stress. In the present data the pigment pool climbed steadily in all treatments, but the reduction between the control and the Eu-doped NPls treated group widened from only 10% at 24 h to 23%, 26% and 29% at 5, 10 and 20 mg L^{-1} after 72 h, respectively (Fig. 5A). The decline runs almost in parallel with the fall in specific growth rate, signifying the inter-relation between growth depression and photosynthesis ability. The behaviour and magnitude of the pigment loss match closely with published NPls exposure studies on freshwater microalgae. For instance, 50 nm PS-NPls were shown to lower Chl-a in *C. vulgaris* by 18–37% over 72 h at concentration between 10–50 mg L^{-1}.[43] Likewise, a 29.64% of Chl-a inhibition rate compared to control was found in *Chlorella pyrenoidosa* after being exposed to 50 mg L^{-1} of 80 nm PS-NPls.[60] These studies support the present observations that NPls can effectively impair Chl-a function through light blockage and internal oxidative damage, resulting in disruptive photosynthesis activity.[59]

The CO_2-fixation assay further confirmed the inhibitory effect of Eu-doped NPls to photosynthesis. The control culture converted 0.055 g biomass L^{-1} d^{-1}, whereas fixation fell to 0.048, 0.046 and 0.044 g biomass L^{-1} d^{-1} at 5, 10 and 20 mg L^{-1} Eu-doped NPls, respectively, implying a cumulative drop of 20% at the highest dose (Fig. 5B). The disturbance in Chl-a function leads to fewer ATP and NADPH availability for processing the Calvin cycle in photosynthesis reaction which resulted in decrease CO_2 fixation rate. Additionally, the pH of the medium during exposure test was recorded and showed a gradual increase from 6.4 to 7.6 in the control, but only to 7.4 in the 20 mg L^{-1} treatment (Fig. S13). The increase of pH is expected, as CO_2 uptake during photosynthesis consumes protons. In aquatic species that rely on a carbon-concentrating mechanism, bicarbonate (HCO_3^-) is actively imported and then converted back to intracellular CO_2 *via* carbonic anhydrase.[61,62] In the presence of Eu-doped NPls as stress-source, slower alkalization in medium reflects to reduced proton consumption. This signifies that less functional pigment corresponding to fewer electrons entering the Calvin cycle, so fewer protons are consumed as CO_2 is hydrated to HCO_3^-, and the medium alkalises more slowly. Similar patterns were also reported by previous study where a dose-dependent fall in CO_2-fixation rate (and glucose output) of *C. vulgaris* exposed to pristine 50 nm PS-NPls down 15–35% between 0.1 and 10 mg L^{-1}.[36]

3.5.2 Reactive oxygen species (ROS) and lipid peroxidation. The oxidative damage arising from NPls chemical reactivity with the cells was detected by measuring the intracellular ROS generation. Over the 72 h exposure period, all treatment groups exhibited a gradual increase in ROS production, correlated positively with increasing Eu-doped NPls concentration and exposure duration (Fig. 5C). At 72 h exposure, the maximum ROS production reached 113.4 ± 9.24%, 117.24 ± 7.9%, and 122.8 ± 1.9% for the 5, 10, and 20 mg L^{-1} groups, respectively, relative to the control. A similar monotonic increase (up to 130% of the control at 50 mg L^{-1}, 72 h) was described for *C. vulgaris* exposed to 50 nm PS-NPls by a recent study,[43] which linked the burst to electron leakage from photosynthetic and respiratory chains when NPls adsorb to the cell. Another study reported an almost identical ROS escalation (20–40% above control) in *Chlamydomonas reinhardtii* during a 96 h exposure to 10–100 mg L^{-1} PS-NPls, underscoring that oxidative stress is a conserved early response across green microalgae.[63] Similarly, ROS escalation has been reported for *Chlorella pyrenoidosa* exposed to 20 nm PS-NPls after 13 days at 50–100 mg L^{-1} where ROS activity rose significantly above the control.[64] The gradual build-up in the present data implying that prolonged particle–cell contact, rather than the initial shading flocs, is the main ROS trigger.

Malondialdehyde (MDA) is a three-carbon dialdehyde produced when poly-unsaturated fatty acids (PUFAs) in biological membranes undergo free-radical chain oxidation. Because each propagation step both amplifies the radical load and consumes an additional PUFA, the amount of MDA formed is directly proportional to the extent of lipid peroxidation, making it a widely accepted quantitative biomarker of oxidative membrane damage.[65,66] In the present experiment, MDA production followed a comparable trend with ROS generation. As seen in Fig. 5D, MDA concentrations rose from 4 mmol/10^6 cells in the control to 6 mmol at 24 h and 15 mmol at 72 h under 20 mg L^{-1} Eu-doped NPls, almost 2.5-fold increase. The coupling is expected, excess ROS initiates the PUFA chain reaction, and the resulting MDA can diffuse and form cross-links with proteins or DNA, compounding cellular stress.[67] Additionally, FTIR analysis of biomass at the end of observation revealed emergence of a new carbonyl shoulder at 1720 cm^{-1} which may be assigned to oxidised lipids or newly formed –COOH groups on photo-aged PS, strengthens with dose, in line with the elevated ROS and MDA levels (Fig. S14).

4. Environmental implications

In real aquatic systems, NPls exposure is inherently dynamic and heterogeneous, shaped by spatial patchiness, varied concentration hotspot, and biological activity.[68–70] Our results show that NPls association with *C. vulgaris* is not static but evolves through the combined effects of encounter frequency, biological feed-backs, and population growth, offering insight into how exposure may unfold in natural environments. Specifically, increasing NPls concentrations elevated the probability of cell–particle encounters while simultaneously stimulating soluble EPS secretion and compositional shifts, indicating a concentration-dependent biological response that can modify particle behaviour and local exposure conditions.

Soluble EPS production introduces a key feedback mechanism where protein-rich soluble EPS may enhance transient particle retention and aggregation within the cellular microenvironment, increasing effective exposure for

a subset of cells, while EPS-mediated aggregation and restabilisation may reduce particle availability for others, as demonstrated in our results as well as other studies.[70–72] This dual role contributes to the dynamic and heterogeneous association patterns resolved by single-cell analysis. Importantly, our observations also indicate that population growth and cell division dilute per-cell NPls burdens over time, as particles may redistributed among daughter cells. Such growth dilution can reduce the average cellular burden even when particles persist in the surrounding medium, partially masking exposure if only bulk metrics are considered. Comparably, quantitative evidence from plant systems further indicates that NPls burdens can be decoupled from external concentrations due to biological modulation and organisms responses, reinforcing the need to consider dynamic exposure rather than static dose assumptions.[73]

In real-world systems, these processes likely operate simultaneously. During algal blooms or periods of rapid primary production, growth dilution may lower mean cellular burdens, as also demonstrated for others aquatic contaminant dynamic.[74,75] However, our results suggest that high-burden subpopulations can persist, driven by repeated encounters or EPS-mediated retention. Thus, temporal exposure peaks such as those occurring near wastewater discharges, resuspension events, or convergence zones,[76–78] may generate transient but ecologically relevant subpopulations experiencing elevated stress, even as the overall population continues to grow. This implies that environmental risk is governed not solely by external NPls concentrations, but by the interplay between exposure intensity, organismal responses (such as soluble EPS secretion), and population dynamics.

Beyond the ecological insights, this study also demonstrates the value of single-cell analytical approaches for environmental NPl research. Conventional bulk measurements typically assume uniform exposure across populations, which can obscure the presence of highly exposed subpopulations that disproportionately contribute to biological effects. By integrating SC-ICP-MS with GMM, this approach enables the resolution of heterogeneous exposure patterns at the individual-cell level, providing a more realistic representation of how NPls interact with microbial communities in natural systems. Such analytical frameworks may therefore help bridge the gap between laboratory observations and environmental complexity by capturing stochastic and heterogeneous exposure processes that are otherwise hidden in population-averaged measurements.

Together, our findings indicate that NPls impacts in natural systems emerge from coupled physical–biological processes, where encounter-driven association, soluble EPS-mediated feed-backs, and growth dilution jointly shape exposure distributions. Accounting for these interacting mechanisms is therefore essential for translating laboratory observations to realistic environmental scenarios and for improving ecological risk assessments of NPls.

5. Conclusion

This study establishes a quantitative framework for deciphering the cell-level heterogeneity underlying NPls toxicity in microalgae. By using Eu as tracer and coupling SC-ICP-MS with unsupervised GMM and GLM, this study resolved the dynamic subpopulations of *C. vulgaris* cells exhibiting variable association with Eu-doped NPls. This analytical workflow enables the identification of heterogeneous exposure patterns that cannot be captured by conventional bulk measurements. The modelling results suggested that a minority of highly burdened cells may contribute disproportionately to overall growth inhibition, offering one possible explanation for inconsistencies often observed in bulk toxicity assays.

Synchrotron nano-XRF imaging further provided spatial evidence consistent with particle localisation within or closely associated with algal cells, while complementary biochemical markers confirmed associated cellular stress responses. These observations suggest that NPl toxicity emerges from heterogeneous and time-dependent cell–particle interactions, rather than uniform exposure across population. However, it should be noted that quadrupole-based SC-ICP-MS is limited to sequential elemental detection, which restricts simultaneous observation of tracer elements and endogenous cellular metals within the same event. Emerging approaches such as inductively coupled plasma time-of-flight mass spectrometry (ICP-TOF-MS), which enable multi-element detection at the single-cell level, may further expand the capability to investigate nanoparticle–cell interactions in future studies. Integrating these emerging analytical tools with statistical frameworks such as the GMM-based approach developed here may further advance the mechanistic understanding of NPl exposure and toxicity in complex environmental systems.

Author contributions

Rega Permana: writing – original draft, methodology, investigation, formal analysis, data curation, conceptualisation. Swati Sharma: writing, review & editing – methodology, investigation, data curation. Bashiru Ibrahim: writing, review & editing – methodology, investigation. Tajudeen A. Oyehan: writing review & editing – investigation. Christopher Stark: writing – review & editing, investigation, validation. Miguel A. Gomez-Gonzalez: writing – review & editing, investigation, validation. Christian Pfrang: writing – review & editing, investigation, validation. Eugenia Valsami-Jones: writing – review & editing, validation, conceptualisation, supervision.

Conflicts of interest

The authors declare that they have no known competing financial interests or personal relationships that could have appeared to influence the work reported in this paper.

Data availability

The authors confirm that all the data supporting the findings of this study are included within the article and its supplementary information (SI). Additional data are available from the corresponding authors upon reasonable request.

Supplementary information is available. See DOI: https://doi.org/10.1039/d6en00046k.

Acknowledgements

RP would like to acknowledge the Indonesia's Education Scholarship (BPI) from The Centre for Higher Education Funding and Assessment (PPAPT), the Ministry of Higher Education, Science and Technology of the Republic of Indonesia, and the Indonesian Endowment Fund for Education (LPDP), for its financial support (Ref. Number 3277/BPPT/BPI.LG/V/2024). SS acknowledges European Union's Horizon 2020 research and innovation program under the Marie Skłodowska-Curie grant (EP/Y016599/1). EVJ acknowledges a Royal Society Wolfson Fellowship (RSWF \R2\192007). The authors acknowledge the Diamond Light Source (United Kingdom) for granting beamtime at the I14 beamline under proposal MG38439.

References

1 J. Gigault, A. Ter Halle, M. Baudrimont, P.-Y. Pascal, F. Gauffre, T.-L. Phi, H. El Hadri, B. Grassl and S. Reynaud, Current opinion: what is a nanoplastic?, *Environ. Pollut.*, 2018, **235**, 1030–1034.

2 N. P. Ivleva, Chemical analysis of microplastics and nanoplastics: challenges, advanced methods, and perspectives, *Chem. Rev.*, 2021, **121**, 11886–11936.

3 Z. Sobhani, X. Zhang, C. Gibson, R. Naidu, M. Megharaj and C. Fang, Identification and visualisation of microplastics/nanoplastics by Raman imaging (i): Down to 100 nm, *Water Res.*, 2020, **174**, 115658.

4 J. J. Alava, A. Jahnke, M. Bergmann, G. V. Aguirre-Martínez, L. Bendell, P. Calle, G. A. Domínguez, E. M. Faustman, J. Falman, T. N. Kazmiruk, N. Klasios, M. T. Maldonado, K. McMullen, M. Moreno-Báez, G. Öberg, Y. Ota, D. Price, W. J. Shim, A. Tirapé, J. M. Vandenberg, Z. Zoveidadianpour and J. Weis, A Call to Include Plastics in the Global Environment in the Class of Persistent, Bioaccumulative, and Toxic (PBT) Pollutants, *Environ. Sci. Technol.*, 2023, **57**, 8185–8188.

5 L. P. Munoz, A. G. Baez, D. Purchase, H. Jones and H. Garelick, Release of microplastic fibres and fragmentation to billions of nanoplastics from period products: preliminary assessment of potential health implications, *Environ. Sci.: Nano*, 2022, **9**, 606–620.

6 S. Fraissinet, G. E. De Benedetto, C. Malitesta, R. Holzinger and D. Materić, Microplastics and nanoplastics size distribution in farmed mussel tissues, *Commun. Earth Environ.*, 2024, **5**, 128.

7 L. J. Hazeem, G. Yesilay, M. Bououdina, S. Perna, D. Cetin, Z. Suludere, A. Barras and R. Boukherroub, Investigation of the toxic effects of different polystyrene micro-and nanoplastics on microalgae Chlorella vulgaris by analysis of cell viability, pigment content, oxidative stress and ultrastructural changes, *Mar. Pollut. Bull.*, 2020, **156**, 111278.

8 W. Yang, P. Gao, G. Ma, J. Huang, Y. Wu, L. Wan, H. Ding and W. Zhang, Transcriptome analysis of the toxic mechanism of nanoplastics on growth, photosynthesis and oxidative stress of microalga Chlorella pyrenoidosa during chronic exposure, *Environ. Pollut.*, 2021, **284**, 117413.

9 C. Schwaferts, R. Niessner, M. Elsner and N. P. Ivleva, Methods for the analysis of submicrometer-and nanoplastic particles in the environment, *TrAC, Trends Anal. Chem.*, 2019, **112**, 52–65.

10 F. A. Monikh, M. G. Vijver, D. M. Mitrano, H. A. Leslie, Z. Guo, P. Zhang, I. Lynch, E. Valsami-Jones and W. J. Peijnenburg, The analytical quest for sub-micron plastics in biological matrices, *Nano Today*, 2021, **41**, 101296.

11 M. Sioen, H. De Keersmaecker, M. Vercauteren, C. Janssen and J. Asselman, Visualization of labeled micro-and nanoplastics in interaction with algae, using super-resolution stimulated emission depletion microscopy and fluorescence lifetime imaging, *Environ. Toxicol. Chem.*, 2025, **44**(3), 624–632.

12 K. D. Sullivan and V. Gugliada, Fluorescence photobleaching of microplastics: a cautionary tale, *Mar. Pollut. Bull.*, 2018, **133**, 622–625.

13 N. K. Mogha and D. Shin, Nanoplastic detection with surface enhanced Raman spectroscopy: Present and future, *TrAC, Trends Anal. Chem.*, 2023, **158**, 116885.

14 F. A. Monikh, L. Chupani, M. G. Vijver and W. J. Peijnenburg, Parental and trophic transfer of nanoscale plastic debris in an assembled aquatic food chain as a function of particle size, *Environ. Pollut.*, 2021, **269**, 116066.

15 E. C. Bair, Z. Guo, T. L. Richardson and J. R. Lead, Quantification of palladium-labelled nanoplastics algal uptake by single cell and single particle inductively coupled plasma mass spectrometry, *Environ. Chem.*, 2024, **21**(5), EN24011.

16 L. Hendriks, V. M. Kissling, T. Buerki-Thurnherr and D. M. Mitrano, Development of single-cell ICP-TOFMS to measure nanoplastics association with human cells, *Environ. Sci.: Nano*, 2023, **10**, 3439–3449.

17 M. K. Ha, K. H. Chung and T. H. Yoon, Heterogeneity in Biodistribution and Cytotoxicity of Silver Nanoparticles in Pulmonary Adenocarcinoma Human Cells, *Nanomaterials*, 2020, **10**(1), 36.

18 Q. Wu, J. Shi, X. Ji, T. Xia, L. Zeng, G. Li, Y. Wang, J. Gao, L. Yao, J. Ma, X. Liu, N. Liu, L. Hu, B. He, Y. Liang, G. Qu and G. Jiang, Heterogenous Internalization of Nanoparticles at Ultra-Trace Concentration in Environmental Individual Unicellular Organisms Unveiled by Single-Cell Mass Cytometry, *ACS Nano*, 2020, **14**, 12828–12839.

19 D. Howard, T. Turnbull, P. Wilson, D. J. Paterson, V. Milanova, B. Thierry and I. Kempson, Quantitative Single-Cell Comparison of Sensitization to Radiation and a Radiomimetic Drug for Diverse Gold Nanoparticle Coatings, *Small Sci.*, 2024, **4**, 2400053.

20 D. A. Reynolds, Gaussian mixture models, *Encyclopedia of biometrics*, 2009, vol. 741, p. 3.
21 Y. Li, X. Wang, D. Liang, X. Zhao, Z. Dong, Y. Bai, W.-X. Wang, W. J. Peijnenburg, Y. Wang and W. Fan, Modelling the size distribution and bioaccumulation of gold nanoparticles under mixture exposure, *Aquat. Toxicol.*, 2025, 107286.
22 M. P. Mulè, A. J. Martins and J. S. Tsang, Normalizing and denoising protein expression data from droplet-based single cell profiling, *Nat. Commun.*, 2022, **13**, 2099.
23 M. Kuroda, A. Isobe, K. Uchida, T. Tokai, T. Kitakado, M. Yoshitake, Y. Miyamoto, T. Mukai, K. Imai and K. Shimizu, Abundance and potential sources of floating polystyrene foam macro-and microplastics around Japan, *Sci. Total Environ.*, 2024, **925**, 171421.
24 Y. Li, S. Liu, Z. Ji, J. Sun and X. Liu, Distinct responses of Chlorella vulgaris upon combined exposure to microplastics and bivalent zinc, *J. Hazard. Mater.*, 2023, **442**, 130137.
25 C. Liang, H. Lv, W. Liu, Q. Wang, X. Yao, X. Li, Z. Hu, J. Wang, L. Zhu and J. Wang, Mechanism of the adverse outcome of Chlorella vulgaris exposure to diethyl phthalate: Water environmental health reflected by primary producer toxicity, *Sci. Total Environ.*, 2024, **912**, 168876.
26 R. Permana, S. Sharma, C. Stark, D. Price, C. Pfrang and E. Valsami-Jones, Europium-labelled nanopolystyrene as model nanoplastics for environmental fate investigations: Synthesis and optimisation, *Polym. Test.*, 2025, **150**, 108903.
27 OECD, *Test No. 201: Freshwater Alga and Cyanobacteria, Growth Inhibition Test*, Paris, 2011, p. 25.
28 E. Besseling, P. Redondo-Hasselerharm, E. M. Foekema and A. A. Koelmans, Quantifying ecological risks of aquatic micro-and nanoplastic, *Crit. Rev. Environ. Sci. Technol.*, 2019, **49**, 32–80.
29 I. L. Hsiao, F. S. Bierkandt, P. Reichardt, A. Luch, Y.-J. Huang, N. Jakubowski, J. Tentschert and A. Haase, Quantification and visualization of cellular uptake of TiO2 and Ag nanoparticles: comparison of different ICP-MS techniques, *J. Nanobiotechnol.*, 2016, **14**, 50.
30 Z. Meng, L. Zheng, H. Fang, P. Yang, B. Wang, L. Li, M. Wang and W. Feng, Single Particle Inductively Coupled Plasma Time-of-Flight Mass Spectrometry—A Powerful Tool for the Analysis of Nanoparticles in the Environment, *Processes*, 2023, 1237.
31 Z. Szymańska, M. Matczuk, A. Żuchowska, P. Romańczuk, A. R. Timerbaev and M. Jarosz, Differentiation of cisplatin uptake within a population of cancer cells – how to "crack this nut" using single-cell ICP-MS, *Analyst*, 2025, **150**, 5374–5378.
32 S. Meyer, A. López-Serrano, H. Mitze, N. Jakubowski and T. Schwerdtle, Single-cell analysis by ICP-MS/MS as a fast tool for cellular bioavailability studies of arsenite, *Metallomics*, 2018, **10**, 73–76.
33 P. D. Quinn, L. Alianelli, M. Gomez-Gonzalez, D. Mahoney, F. Cacho-Nerin, A. Peach and J. E. Parker, The hard X-ray nanoprobe beamline at diamond light source, *J. Synchrotron Radiat.*, 2021, **28**, 1006–1013.
34 V. A. Solé, E. Papillon, M. Cotte, P. Walter and J. Susini, A multiplatform code for the analysis of energy-dispersive X-ray fluorescence spectra, *Spectrochim. Acta, Part B*, 2007, **62**, 63–68.
35 S. Tang, Y. Liu, J. Zhu, X. Cheng, L. Liu, K. Hammerschmidt, J. Zhou and Z. Cai, Bet hedging in a unicellular microalga, *Nat. Commun.*, 2024, **15**, 2063.
36 Z. Sun, S. Zhang, T. Zheng, C. He, J. Xu, D. Lin and L. Zhang, Nanoplastics inhibit carbon fixation in algae: The effect of aging, *Heliyon*, 2024, **10**(8), e29814.
37 F. Rezvani and A. Farazmand, Optimizing light/dark cycles and nutrient ratios for continuous microalgae application in nitrate removal and CO2 fixation, *Int. J. Environ. Sci. Technol.*, 2025, 1–12.
38 L. J. Hazeem, G. Kuku, E. Dewailly, C. Slomianny, A. Barras, A. Hamdi, R. Boukherroub, M. Culha and M. Bououdina, Toxicity effect of silver nanoparticles on photosynthetic pigment content, growth, ROS production and ultrastructural changes of microalgae Chlorella vulgaris, *Nanomaterials*, 2019, **9**, 914.
39 S. E. Sabatini, Á. B. Juárez, M. R. Eppis, L. Bianchi, C. M. Luquet and M. d. C. Ríos de Molina, Oxidative stress and antioxidant defenses in two green microalgae exposed to copper, *Ecotoxicol. Environ. Saf.*, 2009, **72**, 1200–1206.
40 S. Giri and A. Mukherjee, Ageing with algal EPS reduces the toxic effects of polystyrene nanoplastics in freshwater microalgae Scenedesmus obliquus, *J. Environ. Chem. Eng.*, 2021, **9**, 105978.
41 C. L. Kielkopf, W. Bauer and I. L. Urbatsch, Bradford assay for determining protein concentration, *Cold Spring Harb. Protoc.*, 2020, **2020**(4), 102269.
42 T. Masuko, A. Minami, N. Iwasaki, T. Majima, S.-I. Nishimura and Y. C. Lee, Carbohydrate analysis by a phenol–sulfuric acid method in microplate format, *Anal. Biochem.*, 2005, **339**, 69–72.
43 Q. Xiang, Y. Zhou and C. Tan, Toxicity effects of polystyrene nanoplastics with different sizes on freshwater microalgae Chlorella vulgaris, *Molecules*, 2023, **28**, 3958.
44 F. M. Arellano, C. G. L. A. Arcadio, Y.-T. Chen, S. Hsieh, H. P. Bacosa and S.-L. Hsieh, Nanoplastics in biological systems: What laboratory mechanisms reveal about real-world toxicity, *J. Hazard. Mater.*, 2026, **505**, 141464.
45 A. Laycock, N. J. Clark, R. Clough, R. Smith and R. D. Handy, Determination of metallic nanoparticles in biological samples by single particle ICP-MS: a systematic review from sample collection to analysis, *Environ. Sci.: Nano*, 2022, **9**, 420–453.
46 R. Wang, X. Li, J. Li, W. Dai and Y. Luan, Bacterial interactions with nanoplastics and the environmental effects they cause, *Fermentation*, 2023, **9**, 939.
47 F. A. Monikh, L. Chupani, Z. Guo, P. Zhang, G. K. Darbha, M. G. Vijver, E. Valsami-Jones and W. J. Peijnenburg, The stochastic association of nanoparticles with algae at the cellular level: Effects of NOM, particle size and particle shape, *Ecotoxicol. Environ. Saf.*, 2021, **218**, 112280.

48 J. Bourquin, D. Septiadi, D. Vanhecke, S. Balog, L. Steinmetz, M. Spuch-Calvar, P. Taladriz-Blanco, A. Petri-Fink and B. Rothen-Rutishauser, Reduction of Nanoparticle Load in Cells by Mitosis but Not Exocytosis, *ACS Nano*, 2019, **13**, 7759–7770.

49 E. Brynzak-Schreiber, E. Schögl, C. Bapp, K. Cseh, V. Kopatz, M. A. Jakupec, A. Weber, T. Lange, J. L. Toca-Herrera, G. del Favero, W. Wadsak, L. Kenner and V. Pichler, Microplastics role in cell migration and distribution during cancer cell division, *Chemosphere*, 2024, **353**, 141463.

50 P. M. Perrigue, A. Henschke, B. F. Grześkowiak, Ł. Przysiecka, K. Jaskot, A. Mielcarek, E. Coy and S. E. Moya, Cellular uptake and retention studies of silica nanoparticles utilizing senescent fibroblasts, *Sci. Rep.*, 2023, **13**, 475.

51 F. Abdolahpur Monikh, L. Chupani, D. Arenas-Lago, Z. Guo, P. Zhang, G. K. Darbha, E. Valsami-Jones, I. Lynch, M. G. Vijver and P. M. van Bodegom, Particle number-based trophic transfer of gold nanomaterials in an aquatic food chain, *Nat. Commun.*, 2021, **12**, 899.

52 S. Patel and A. Green, Death by p-value: the overreliance on p-values in critical care research, *Crit. Care*, 2025, **29**, 73.

53 S. R. Vinceti and T. Filippini, Towards the dismissal of null hypothesis/statistical significance testing in public health, public law and toxicology, *Public Health Toxicol.*, 2021, **1**, 1–6.

54 M. K. Ha, J.-S. Choi, S. J. Kwon, J. Song, Y. Lee, Y.-E. Kim and T. H. Yoon, Mass cytometric study on the heterogeneity in cellular association and cytotoxicity of silver nanoparticles in primary human immune cells, *Environ. Sci.: Nano*, 2020, **7**(4), 1102–1114.

55 S. Sala, K. Rengefors, J. Kiventerä, M. Patanen, L. Gefors, C. Werdinius, S. Winge, K. Broberg, S. Kalbfleisch and K. Sigfridsson Clauss, Applications of X-ray fluorescence microscopy with synchrotron radiation: From biology to materials science, *Radiat. Phys. Chem.*, 2025, **229**, 112491.

56 A. J. Specht, X. Zhang, O. A. Antipova, A. S. M. Sayam, V. T. Nguyen, C. G. Hoover, T. Punshon, B. P. Jackson and M. G. Weisskopf, Sub-micrometer scale synchrotron x-ray fluorescence measurements of trace elements in teeth compared with laser ablation inductively coupled plasma mass spectrometry, *J. Exposure Sci. Environ. Epidemiol.*, 2025, **35**, 625–629.

57 S. Vasilieva, O. Gorelova, O. Baulina and E. Lobakova, Subcellular localization of manganese in two green microalgae species with different tolerance to elevated Mn concentrations, *Russ. J. Plant Physiol.*, 2022, **69**, 94.

58 M. Plouviez, B. Guieysse, K. Wolmarans, A. M. E. Matinong, O. Buwalda, K. Thånell, I. Beinik, J. R. M. Tuyishime, V. Mitchell, P. Kappen, D. Flynn, T. Jauffrais and R. G. Haverkamp, Microalgae for the Extraction and Separation of Rare Earths: An STXM Study of Ce, Gd, and P, *ACS Sustainable Resour. Manage.*, 2024, **1**, 2225–2233.

59 X. Li, H. Qiu, P. Zhang, L. Song, A. Romero-Freire and E. He, Role of heteroaggregation and internalization in the toxicity of differently sized and charged plastic nanoparticles to freshwater microalgae, *Environ. Pollut.*, 2023, **316**, 120517.

60 W. Yang, P. Gao, H. Li, J. Huang, Y. Zhang, H. Ding and W. Zhang, Mechanism of the inhibition and detoxification effects of the interaction between nanoplastics and microalgae Chlorella pyrenoidosa, *Sci. Total Environ.*, 2021, **783**, 146919.

61 S. Zerveas, M. S. Mente, D. Tsakiri and K. Kotzabasis, Microalgal photosynthesis induces alkalization of aquatic environment as a result of H+ uptake independently from CO2 concentration–New perspectives for environmental applications, *J. Environ. Manage.*, 2021, **289**, 112546.

62 K. Gao, Approaches and involved principles to control pH/pCO2 stability in algal cultures, *J. Appl. Phycol.*, 2021, **33**, 3497–3505.

63 X. Li, Z. Chu, C. Feng, P. Song, T. Yang, L. Zhou, X. Zhao, X. Chai, J. Xing and S. Chen, Unveiling the molecular mechanisms of size-dependent effect of polystyrene micro/nano-plastics on Chlamydomonas reinhardtii through proteomic profiling, *Chemosphere*, 2024, **358**, 142220.

64 Z. Guo, T. Chen, M. Wang and M. Qin, Size-Dependent Effects of Polystyrene Nanoplastics on Freshwater Microalgae After Long-Term Exposure, *Water*, 2025, **17**, 655.

65 S. Gaweł, M. Wardas, E. Niedworok and P. Wardas, Malondialdehyde (MDA) as a lipid peroxidation marker, *Wiad. Lek.*, 2004, **57**, 453–455.

66 P. Singh, S. Singh, P. Maurya, A. Mohanta, H. Dubey, S. R. Khadim, A. K. Singh, A. K. Pandey, A. K. Singh and R. K. Asthana, Bioaccumulation of selenium in halotolerant microalga Dunaliella salina and its impact on photosynthesis, reactive oxygen species, antioxidative enzymes, and neutral lipids, *Mar. Pollut. Bull.*, 2023, **190**, 114842.

67 L. J. Marnett, Lipid peroxidation—DNA damage by malondialdehyde, *Mutat. Res., Fundam. Mol. Mech. Mutagen.*, 1999, **424**, 83–95.

68 S. A. Forrest, D. McMahon, W. A. Adams and J. C. Vermaire, Change in microplastic concentration during various temporal events downstream of a combined sewage overflow and in an urban stormwater creek, *Front. Water*, 2022, **4**, 958130.

69 R. Rynek, M. B. Tekman, C. Rummel, M. Bergmann, S. Wagner, A. Jahnke and T. Reemtsma, Hotspots of Floating Plastic Particles across the North Pacific Ocean, *Environ. Sci. Technol.*, 2024, **58**, 4302–4313.

70 S. Xiong, X. Cao, I. Eggleston, Y. Chi, A. Li, X. Liu, J. Zhao and B. Xing, Role of extracellular polymeric substances in the aggregation and biological response of micro(nano) plastics with different functional groups and sizes, *J. Hazard. Mater.*, 2023, **446**, 130713.

71 L. Natarajan, S. Omer, N. Jetly, M. A. Jenifer, N. Chandrasekaran, G. K. Suraishkumar and A. Mukherjee, Eco-corona formation lessens the toxic effects of polystyrene nanoplastics towards marine microalgae Chlorella sp, *Environ. Res.*, 2020, **188**, 109842.

72 R.-F. Shiu, C. I. Vazquez, C.-Y. Chiang, M.-H. Chiu, C.-S. Chen, C.-W. Ni, G.-C. Gong, A. Quigg, P. H. Santschi and W.-C. Chin, Nano- and microplastics trigger secretion of protein-rich extracellular polymeric substances from phytoplankton, *Sci. Total Environ.*, 2020, **748**, 141469.

73 Y. Wang, F. Wang, L. Xiang, M. Liao, M. Wang, Y. Bian, X. Jiang, R. Naidu, M. C. Rillig and W. Amelung, Co-exposure of di(2-ethylhexyl) phthalate (DEHP) decreased the submicron plastic stress in soil–plant system, *Eco-Environ. & Health*, 2025, **4**, 100184.

74 E. J. Petersen, M. Mortimer, R. M. Burgess, R. Handy, S. Hanna, K. T. Ho, M. Johnson, S. Loureiro, H. Selck, J. J. Scott-Fordsmand, D. Spurgeon, J. Unrine, N. W. van den Brink, Y. Wang, J. White and P. Holden, Strategies for robust and accurate experimental approaches to quantify nanomaterial bioaccumulation across a broad range of organisms, *Environ. Sci.: Nano*, 2019, **6**, 1619–1656.

75 Y. Zheng and B. Nowack, Comparison of biokinetic models for non-dissolvable engineered nanomaterials in freshwater aquatic organisms, *Environ. Sci.: Nano*, 2023, **10**, 1065–1076.

76 A. Asadi, F. Khodadoost, N. Daglioglu and S. Eris, A systematic review on the occurrence and removal of microplastics during municipal wastewater treatment plants, *Environ. Eng. Res.*, 2025, **30**(2), 240366.

77 T. L. Jolaosho, M. F. Rasaq, E. V. Omotoye, O. V. Araomo, O. S. Adekoya, O. Y. Abolaji and J. J. Hungbo, Microplastics in freshwater and marine ecosystems: Occurrence, characterization, sources, distribution dynamics, fate, transport processes, potential mitigation strategies, and policy interventions, *Ecotoxicol. Environ. Saf.*, 2025, **294**, 118036.

78 M. Nakakuni, M. Nishida, R. Nishibata, K. Kishimoto, H. Yamaguchi, K. Ichimi, M. Ishizuka, Y. Suenaga and K. Tada, Convergence zones of coastal waters as hotspots for floating microplastic accumulation, *Mar. Pollut. Bull.*, 2024, **206**, 116691.

